

## Subsurface defect detection using phase evolution of line laser-generated Rayleigh waves

Dan Chen<sup>1,2,3,†</sup>, Gaolong Lv<sup>1,2,3,†</sup>, Shifeng Guo<sup>1,2,3,a)</sup>, Rui Zuo<sup>1,2,3</sup>, Yanjun Liu<sup>4</sup>, Kaixing Zhang<sup>5</sup>, Zhongqing Su<sup>6</sup>, Wei Feng<sup>1,2,3</sup>

<sup>1</sup>Shenzhen Key Laboratory of Smart Sensing and Intelligent Systems, Shenzhen Institutes of Advanced Technology, Chinese Academy of Sciences, Shenzhen 518055, China

<sup>2</sup>Guangdong Provincial Key Lab of Robotics and Intelligent System, Shenzhen Institutes of Advanced Technology, Chinese Academy of Sciences, Shenzhen 518055, China

<sup>3</sup>CAS Key Laboratory of Human-Machine Intelligence-Synergy Systems, Shenzhen Institutes of Advanced Technology, Shenzhen 518055, China

<sup>4</sup>Department of Electrical and Electronic Engineering, Southern University of Science and Technology, Shenzhen 518055, China

<sup>5</sup>College of Mechanical and Electronic Engineering, Shandong Agricultural University, Tai'an 271018, China

<sup>6</sup>Department of Mechanical Engineering, The Hong Kong Polytechnic University, Hung Hom, Kowloon, Hong Kong SAR 999077, China

<sup>†</sup>The authors contributed equally to this work.

<sup>a)</sup>Author to whom correspondence should be addressed: sf.guo@siat.ac.cn (S. Guo)

### ABSTRACT

An unreported phenomenon of phase evolution of Rayleigh waves with subsurface defects is observed and systematically explored for detection of subsurface defects using non-contact line laser ultrasonic technique and numerical simulation. The mechanism of phase evolution of Rayleigh wave signals is explained by the interference of the reflected Rayleigh wave and direct Rayleigh wave, explored by finite element analysis. Both experiments and simulation show distinct peak evolution of the Rayleigh wave signals with the width and depth of subsurface defect. A dimensionless parameter ( $|Neg|/Pos$ ), defined by the ratio of absolute negative peak to positive peak of Rayleigh wave, is proposed to evaluate the phase evolution of Rayleigh wave with defect width and depth, which is further used to quantify the subsurface defects. The phase evolution of Rayleigh waves can act as a robust and sensitive feature to detect subsurface defects using laser-generated ultrasound, which has promising applications in life prediction and health monitoring of various engineering structures.

*Key words:*

Rayleigh wave; Laser ultrasonics; Subsurface defects; Phase evolution; Nondestructive evaluation

### 1. Introduction

The subsurface defect hidden beneath the surface of structure is detrimental to the strength, performance and lifetime of critical structure and may cause catastrophic accidents if not detected in advance[1-3]. In particular, for the additive manufactured structures, the interlayer defects, such as pores, inclusions and cracks, are inevitably introduced and difficult to be detected in-situ by conventional detection methods[4-6]. A reliable nondestructive evaluation (NDE) technique that enables the detection and evaluation of subsurface defects in safety-critical structures is therefore highly demanded. Ultrasonic inspection has received considerable attention for identifying internal and subsurface defects of various structures[7-10]. However, conventional ultrasonic NDE techniques are generally contact-based and require additional coupling agent, fixtures for generation and detection of ultrasonic signals[11-18], which are not applicable in harsh environment (high temperature, serious radiation, etc.) and for complicated structures.

Laser ultrasound (LU) is a technique that based on ther-

mo-elastic or ablation mechanism to generate ultrasonic waves and using interferometer to detect surface displacement of structures[19-21]. LU with the advantages of non-contact generation and detection, broad bandwidth reception, accessibility for harsh environments and complex structures, has been implemented for inspecting structural materials with various defects[20, 22-25]. The laser-generated Rayleigh waves that propagate along the surface of structures are more sensitive to detect surface-breaking cracks or subsurface defects than bulk longitudinal wave and shear wave[26-29].

The interaction of laser-generated Rayleigh wave with surface-breaking cracks has been studied using thermoelastic model, numerical simulation and scanning laser source (SLS) technique, and the signal characteristics, such as transmission and reflection coefficients[20], amplitude and frequency content[30] of the Rayleigh waves were used to detect defects. The laser generated ultrasonic waves were also reported to detect internal or subsurface surface defects by analyzing the features of velocity dispersion[31] time-of-flight, time-domain signal amplitude, spectrum distribution[32]. The above men-

tioned laser ultrasonic methods have limitations in low detection sensitivity, weak robustness, and require reference parameters for comparison, therefore are difficult to be applied in real applications.

This paper presents a systematic study of the interaction of pulsed line laser-generated Rayleigh waves with subsurface defects, and a new method to detect subsurface defects is proposed. The phase evolution, an unreported phenomenon, which shows the transformation of Rayleigh wave peak with the presence of subsurface defects are explored experimentally and numerically. A dimensionless parameter  $|Neg|/Pos$  is proposed to quantitatively describe the relationship between phase evolution and defect depth and size. The phase evolution of Rayleigh waveforms can be adopted as a reliable and sensitive feature to evaluate and monitor the structure integrity.

## 2. Pulsed-laser ultrasonic experiment

### 2.1. Experimental details

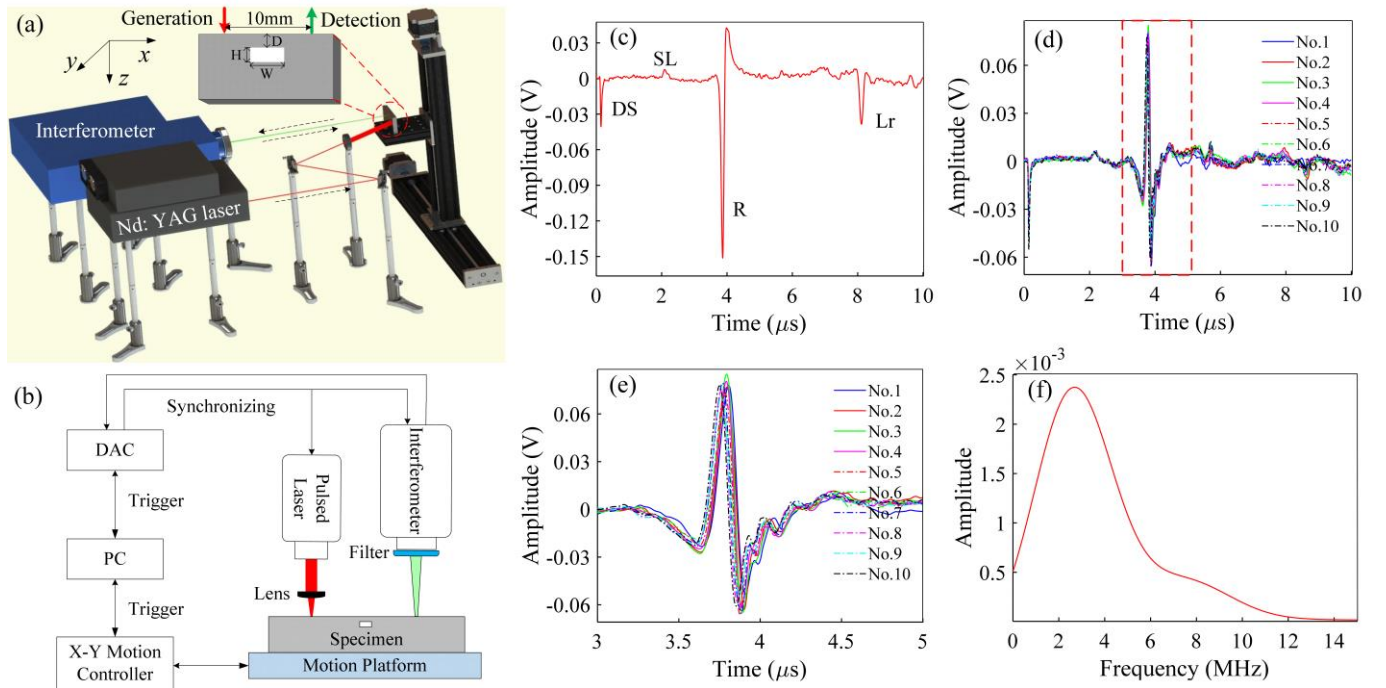


**Fig. 1.** The Rayleigh ultrasonic waves generated by a pulsed laser in stainless-steel specimens. (a) The configuration of experimental setup. H, D and W are abbreviations of the height, depth and width of subsurface defect, respectively. (b) The schematic of the experimental setup for detecting subsurface defects with ultrasonic waves excited by pulsed laser and detected by a double-wave mixed interferometer. (c) The representative Rayleigh ultrasonic waves from specimen without defect. DS, SL, R and Lr are abbreviations of disturbance signal, skimming longitudinal wave, Rayleigh wave, and reflected longitudinal wave, respectively. (d) The Rayleigh wave signals received from specimen with defect dimension H, D, W of 1.0, 0.5 and 1.5 mm, obtained from 10 different positions along the y-axis. (e) The zoomed signals in (d) (identified by the dash line) shows excellent consistency of Rayleigh wave signals. (f) The representative frequency spectrum of Rayleigh wave from (e).

Both the pulsed line laser source and the interferometer are kept at 5 mm away from the center of defects, with a distance of 10 mm in x direction for all specimens. The acquired signals are digitized by a high-resolution data acquisition card (DAC) with 12-bit sampling depth, and averaged 200 times to improve the signal-to-noise ratio [Fig. 1(b)]. To exclude any effect from surface roughness, the

The experimental setup is shown in Fig. 1(a). A Nd:YAG pulsed laser (Centurion+) with wavelength of 1064 nm, pulse duration of 12 ns is used to generate Rayleigh wave under thermoelastic mechanism, which is focused to a line laser source with length of 15 mm and width of 0.5 mm. The double-wave mixed interferometer (TEMPO 2D) with an operating wavelength of 532 nm and a bandwidth of 20 MHz is applied to receive the out-of-plane displacement of Rayleigh ultrasonic waves. A band-pass filter of 532 nm is combined with the interferometer to avoid the generation of disturbance signal by the pulsed laser. For defects with sizes much smaller than the line laser source and far away from the detection point, the effect of orientation and shape of defects to the received Rayleigh wave signals can be ignored[33]. For simplicity, a series of rectangular-shape slits (ARSSs) of fixed height (H) of 1.0 mm, different depth (D) of 0.5, 1.0, 1.5 mm and various width (W) of 0, 0.5, 1.5, 3 mm, are therefore artificially fabricated as subsurface defects for this study.

front surface of all specimens is milled to about 0.8  $\mu\text{m}$ . The representative time-domain signal from specimen free of defect is shown in Fig. 1(c). Under thermoelastic mechanism, three type of waveforms, including, skimming longitudinal wave (SL), Rayleigh wave (R) and reflected longitudinal wave ( $L_r$ ) from the bottom of specimen are identified by the calculated wave velocity. The disturbance signal (DS) is at-

tributed to the system interference.

Fig. 1(d) shows 10 signals obtained from ten different positions along the y-axis, with fixed ARSS dimension H, D, W of 1.0, 0.5, and 1.5 mm, respectively. The zoomed Rayleigh waves in Fig. 1(e) show that the 10 signals have excellence in consistency, indicating the received signal is stable and unaffected by the signal acquisition position. The representative frequency spectrum of Rayleigh wave signal is shown in Fig. 1(f). The central frequency of the generated Rayleigh wave is 3.0 MHz, and the acoustic energy is mainly concentrated in the range of 2-4.5 MHz, with the estimated wavelength from 0.844 to 1.9 mm.

To study the interaction of Rayleigh waves with subsurface defects, a series of specimens with ARSSs at a fixed defect width (W) of 1.0 mm and various depths (D) of 0.5, 1.0, 1.5 mm are prepared for the experiment. For specimen free of subsurface defect, a strong negative peak is observed (pointed by green arrow), with a negligible positive peak (pointed by

red arrow), shown in Fig. 2(a). With the occurrence of an ARSS with depth (D) of 0.5 mm, a strong positive peak occurs, shown in Fig. 2(b). However, the positive peak decreases when the depth of ARSS increases to 1.0 mm, and it reduces substantially as the depth increased to 1.5 mm, shown in Fig. 2(c-d). In contrast, the negative peak decreases at defect depth of 0.5 mm but increases with defect depth. The result indicates that the phase evolution of Rayleigh waves (an obvious positive peak) can act as a robust and sensitive feature to detect subsurface defects, as shown in Fig. 1 (a)-(b). The explanation for the evolved positive peak with defect depth will be analyzed by finite element analysis in the next section. It should be point out that the phase evolution of Rayleigh waves with subsurface defects is unique in line laser source generation and interferometer reception, which is not feasible to be observed using piezoelectric ultrasonic transducers, due to their bandwidth limitations[10, 14].

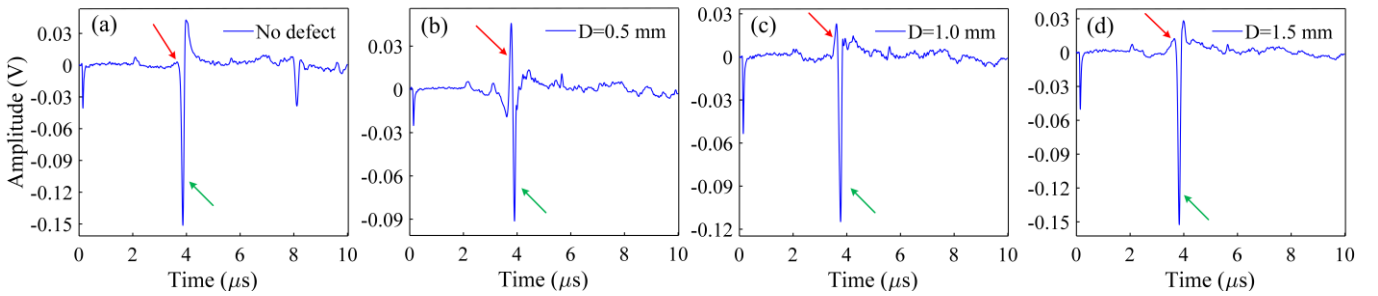


**Fig. 2.** Phase evolution of Rayleigh wave with defect depth. (a) Without defect. (b-d) Subsurface defects depths of 0.5, 1.0, 1.5 mm. The height (H) and width (W) is fixed at 1.0 mm and 1.0 mm, respectively.

## 2.2 Numerical simulation and analysis

In order to explain the phenomenon of phase evolution of Rayleigh wave, a two-dimensional finite element model is established using Comsol Multiphysics 5.4. The thermal stress module is selected to model the interaction of Rayleigh waves with subsurface defects. The governing equations for the coupled temperature and displacement fields is expressed as[34]

$$\nabla^2 T - \frac{1}{\kappa} \dot{T} - \frac{1}{c^2} \ddot{T} = -\frac{q}{k} \quad (1)$$

and

$$\mu \nabla^2 \mathbf{u} + (\lambda + \mu) \nabla (\nabla \cdot \mathbf{u}) = \rho \ddot{\mathbf{u}} + \beta \nabla T \quad (2)$$

where  $T$  is the absolute temperature,  $\mathbf{u}$  the displacement vector field,  $\kappa$  the thermal diffusivity,  $c$  the heat propagation speed which is equal to the longitudinal wave speed,  $k$  the thermal conductivity,  $\beta$  the thermoacoustic coupling constant:  $\beta=(3\lambda+2\mu)\alpha_T$ ,  $\lambda, \mu$  the Lamé constant,  $\alpha_T$  the coefficient of the linear thermal expansion.  $q$  is the heat source due to laser line-source illumination, which has a Gaussian distribution in

$x$ - $z$  plane. The heat flow that has the same parameters as the pulsed laser energy is applied to the top boundary of the model. The function of heat flow is expressed as

$$q = P_0(1-r) \frac{t}{\tau} \exp\left(-\frac{x^2}{\delta^2}\right) \exp\left(-\frac{t}{\tau}\right) \quad (3)$$

where  $P_0$  is the power amplitude,  $r$  the light reflection coefficient,  $\tau$  and  $\delta$  the rise time and line width of the pulsed laser. In addition, low-reflection boundaries are considered on both sides of the model and local mesh refinement is conducted on the top boundary. To observe the wave propagation and interaction between the generated ultrasonic waves and defects, the model is solved using transient solver.

Fig. 3 shows the simulation results of the interaction of laser generated Rayleigh waves with specimens of various defect depths. Four types of waveforms, including the Rayleigh wave (R), shear wave (S), skimming longitudinal wave (SL) and body longitudinal wave (L), are clearly identified by the propagation direction and wave velocity, shown in Fig. 3(a). For the specimen free of defect, the Rayleigh wave has the strongest magnitude compared with other waveforms and

mainly concentrated in the depth less than 2 mm. The Rayleigh wave and skimming longitudinal wave are marked with red and white arrows in inset of Fig. 3(a).

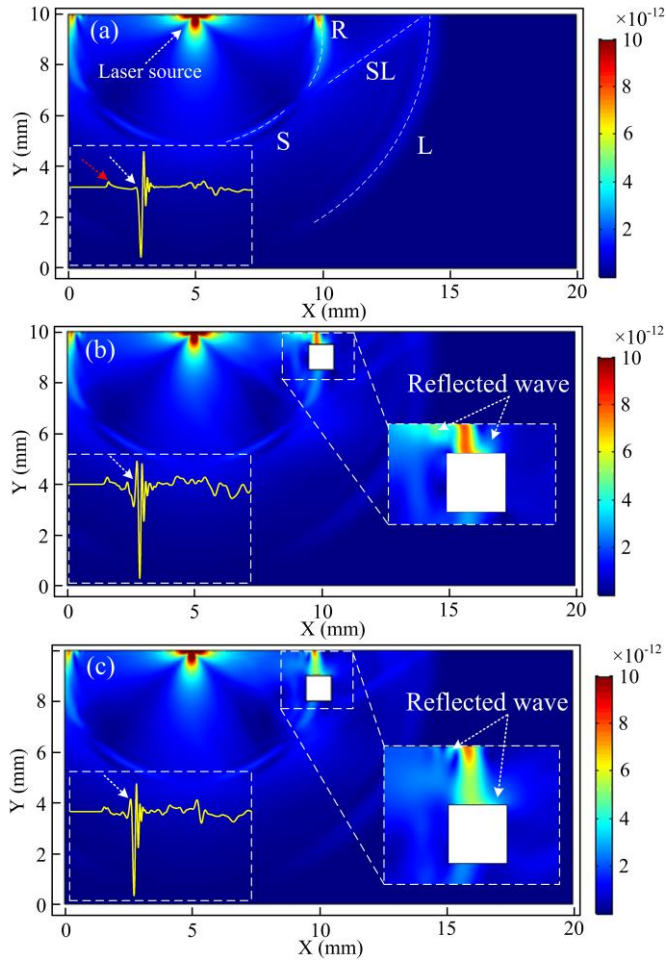


**Fig. 3.** The simulation results of the interaction of laser generated Rayleigh waves with specimens with and without defects. (a) Without defect. (b) Defect depth of 0.5 mm. (c) Defect depth of 1.0 mm. The simulated time-domain signals and the displacement field at each depth are inserted. The height (H) and Width (W) of the defect is kept at 1.0 and 1.0 mm, respectively.

For the subsurface defect with depth (D) of 0.5 mm, an enhanced Rayleigh wave is observed, shown in Fig. 3(b), which is mainly attributed to the superimposition of reflected and direct Rayleigh waves with wavelength larger than 0.5 mm. The presence of the subsurface defect generates a strong positive peak, pointed by the white arrow in inset, which is

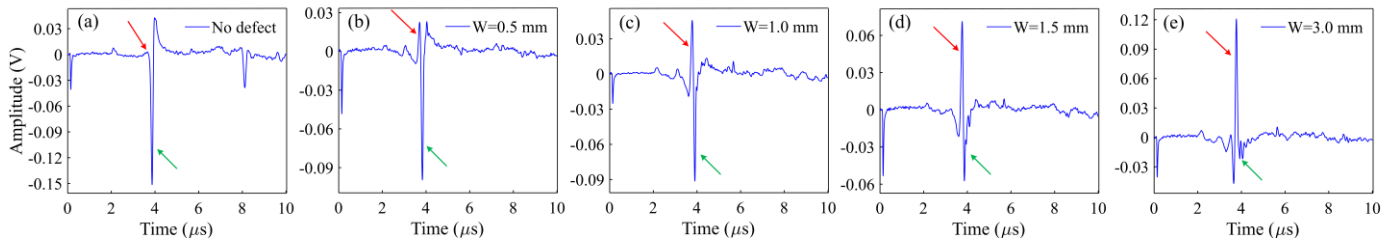


**Fig. 4.** Phase evolution of Rayleigh wave with defect depth. (a) Without defect. (b) Defect width of 0.5 mm. (c-e). Defect width of 1.0, 1.5, 3.0 mm. The height (H) and depth (D) is fixed at 1.0 mm and 0.5 mm, respectively.

According to the pulse duration of Rayleigh wave (Fig.1 (e)), the length of the generated Rayleigh wave along the propagation direction is estimated at 3 mm. Therefore, for

consistent with the experimental results in Fig. 2(b). The phase evolution as a result of the subsurface defect can be explained by the interference of direct and reflected Rayleigh wave, which can act as an obvious indicator for the presence of subsurface defect. The phase change of Rayleigh wave has also been studied to detect surface crack[35], but which is generated mainly by the interaction of near-field surface wave and bulk wave between the source and the defect. Therefore, such method is only applicable to detect localized surface-breaking defects, with limited applications.

As the energy of Rayleigh wave decays exponentially with depth, the reflected Rayleigh wave substantially reduces when the defect depth increases to 1.0 mm. Therefore, the superimposition of reflected and direct Rayleigh waves is reduced [Fig. 3(c)], consequently with a reduced positive peak, shown in inset of Fig. 3(c). The simulation result is consistent well with the experimental result in Fig. 2. Both show a strong evolved positive peak of Rayleigh wave signals at small defect depth of 0.5 mm and a reduced positive peak with larger defect depth.

### 3. Results and discussions

The phase evolution of Rayleigh wave with defect width is further explored, conducted on specimens with fixed defect depth (0.5 mm) and various defect width (0, 0.5, 1.5, and 3 mm). The result in Fig. 4 shows that the evolution of positive peak of Rayleigh wave occurs at defect width of 0.5 mm, and the positive peak increases obviously with defect width, identified by the red arrow, with the value increases linearly from 0 to 0.12 V, summarized in Fig 5. The negative peak of the Rayleigh wave (pointed by green arrow), however, decreases monotonically with defect width, with the value decreases linearly from 0.15 to 0 V, shown in Fig 5. This result shows that the phase evolution of Rayleigh wave is extremely sensitive to the width of subsurface defects.

defect with width of 0.5 mm, part of the reflected Rayleigh wave dissipates during propagation (shown in Fig. 3(b)), and such dissipation effects reduce with defect width and therefore



induces a stronger superimposition of the reflected and direct Rayleigh wave. This may explain the evolved positive peak of the Rayleigh waves is weaker at small defect width and increases with defect width. The result in Fig.4 and Fig. 5 show that the phase of Rayleigh wave changes obviously and monotonically as defect width, suggesting it can be used as a reliable indicator for measuring width of subsurface defects.

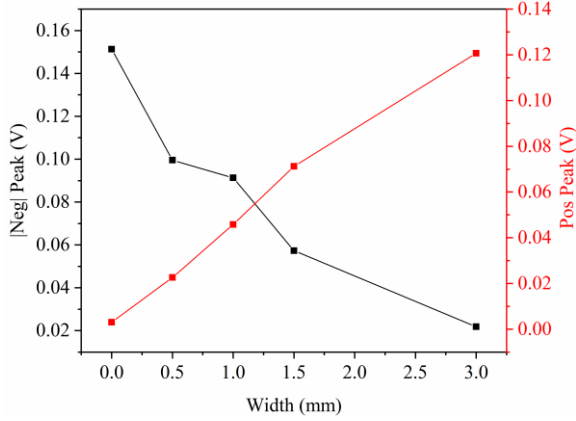


**Fig. 5.** Variation of the |Neg| peak and positive peak of Rayleigh wave with subsurface defect width.

In order to obtain a general law of phase evolution of Rayleigh wave with defect depth and width, specimens with various depths (0.5, 1.0, 1.5 mm) and widths (0.5, 0.8, 1.0, 1.2, 1.5, 2.0, 3.0 mm) are detected, with a total number of 21 specimens. Three characteristic parameters, including the absolute negative peak (|Neg| peak), positive peak (Pos-peak),

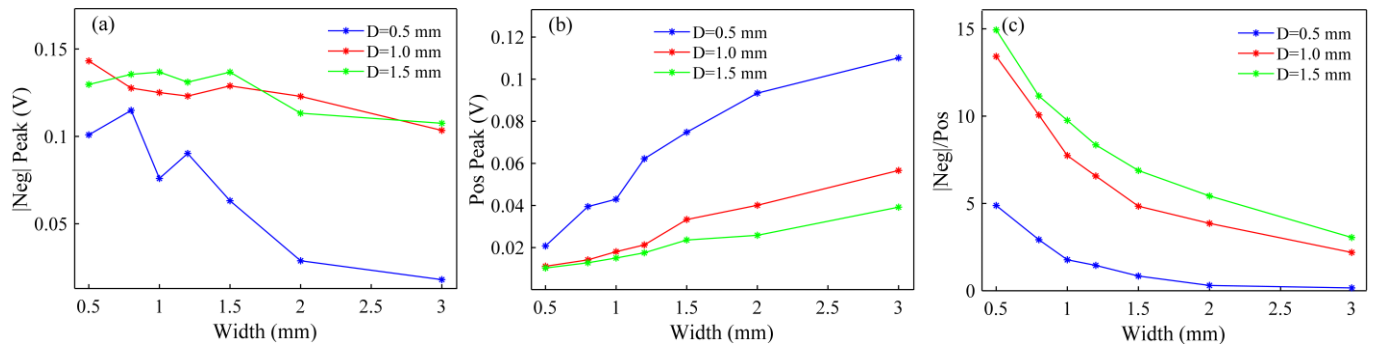


**Fig. 6.** The relationships between characteristic parameters and defect depth and width. (a) |Neg|-peak. (b) Pos-peak. (c) |Neg|/Pos.

The |Neg|/Pos proposed is a dimensionless parameter that eliminates the impact of incident laser energy, material attenuation, and propagation distance on the amplitude of Rayleigh wave. As shown in Fig. 6(c), the |Neg|/Pos parameter decreases monotonically with defect width at evaluated defect depths for three defect depth cases. Therefore the |Neg|/Pos parameter can be acted as an important parameter to quantify the defect width or depth.

#### 4. Conclusion

An unreported phenomenon of phase evolution of Rayleigh waves with subsurface defects is observed and systematically explored using all-optical laser ultrasonic technique

and ratio of absolute negative peak to positive peak ( $|Neg|/Pos$ ), are proposed to describe the phase evolution of Rayleigh wave. Fig. 6(a) shows the relationship between Neg-peak and the defect width and depth. At the fixed defect depth of 0.5 mm, the absolute value of Neg-peak ( $|Neg|$  peak) decreases monotonically with defect width. However, for defect depth of 1.0 and 1.5 mm, the  $|Neg|$  peak does not change substantially with defect width.

Fig. 6(b) shows the relationship between the Pos-peak and defect width and depth. In contrast, the Pos-peak value exhibits a completely opposite trend to that of in Fig. 6(a), which increases monotonically with defect width. Combined with the numerical simulation results in Fig 3, the difference in the slope of  $|Neg|$ -peak curve [Fig. 6(a)] and Pos-peak curve [Fig. 6(b)] with defect depth is attributed to the penetration depth of the Rayleigh wave. While the difference in the slope of  $|Neg|$ -peak curve and Pos-peak curve changed with defect width is attributed to the length of Rayleigh waves. The comparison between Fig. 6(a) and Fig. 6(b) shows the transformation between the negative peak and positive peak of Rayleigh wave, which undoubtedly proves the occurrence of phase evolution and implies the existence of subsurface defects.

and numerical simulation. The phase evolution or even reversal of the Rayleigh wave is attributed to the superposition of the reflected Rayleigh wave and the direct Rayleigh wave with wavelength larger than the defect depth. A dimensionless parameter  $|Neg|/Pos$  is proposed to describe the phase evolution of Rayleigh wave, which presents a monotonically variation trends with defect width and depth. Therefore,  $|Neg|/Pos$  can be used as a reliable parameter to quantify the depth and width of subsurface defects.

#### Author statement

Shifeng Guo supervised the project, conceived the approach, evaluate the results and corrected the manuscript. Dan

Chen implemented the experiments, analyzed the data and wrote the paper. Gaolong Lv prepared and carried out the experiments. Rui Zuo prepared the experimental setup. Yanjun Liu guided the laser ultrasonic experiments. Wei Feng, Kaixing Zhang, and Zhongqing Su made evaluated and commented on the results. Dan Chen and Gaolong Lv contributed equally to this work.

### Acknowledgements

The authors are grateful to the financial support from the National Natural Science Foundation of Guangdong (grant numbers 2016A030313177), Guangdong Frontier and Key Technological Innovation (grant numbers 2017B090910013), the Science and Technology Innovation Commission of Shenzhen (grant numbers ZDSYS20190902093209795, JCYJ20170818153048647 and JCYJ 20180507182239617).

### References

[1] P. Maruschak, O. Prentkovskis, R. Bishchak, Defectiveness of external and internal surfaces of the main oil and gas pipelines after long-term operation, *Journal of Civil Engineering and Management* 22(2) (2016) 279-286.

[2] J. Wu, J. Zhu, H. Xia, C. Liu, X. Huang, G.Y. Tian, DC-biased magnetization based eddy current thermography for subsurface defect detection, *IEEE Transactions on Industrial Informatics* 15(12) (2019) 6252-6259.

[3] J. Ahmad, A. Akula, R. Mulaveesala, H. Sardana, An independent component analysis based approach for frequency modulated thermal wave imaging for subsurface defect detection in steel sample, *Infrared Physics & Technology* 98 (2019) 45-54.

[4] S.K. Everton, M. Hirsch, P. Stravroulakis, R.K. Leach, A.T. Clare, Review of in-situ process monitoring and in-situ metrology for metal additive manufacturing, *Materials & Design* 95 (2016) 431-445.

[5] D. Cerniglia, M. Scafidi, A. Pantano, J. Rudlin, Inspection of additive-manufactured layered components, *Ultrasonics* 62 (2015) 292-298.

[6] C. Millon, A. Vanhoye, A-F. Obaton, J. W. Penot, Development of laser ultrasonics inspection for online monitoring of additive manufacturing, *Ultrasonics* 62(3) (2018) 653-661.

[7] H. Xiao, D. Chen, J. Xu, S. Guo, Defects identification using the improved ultrasonic measurement model and support vector machines, *NDT & E International* (2020) 102223.

[8] V. Zarubin, A. Bychkov, V. Simonova, V. Zhigarkov, A. Karabutov, E. Cherepetskaya, A refraction-corrected tomographic algorithm for immersion laser-ultrasonic imaging of solids with piecewise linear surface profile, *Applied*

*Physics Letters* 112(21) (2018) 214102.

[9] D. Chen, H. Xiao, M. Li, J. Xu, A study on the inclusion sizing using immersion ultrasonic C-scan imaging, *Journal of Physics: Conference Series*, IOP Publishing, 2017, p. 012003.

[10] S. Guo, L. Zhang, S. Chen, C.K.I. Tan, K. Yao, Ultrasonic transducers from thermal sprayed lead-free piezoelectric ceramic coatings for in-situ structural monitoring for pipelines, *Smart Materials and Structures* 28(7) (2019) 075031.

[11] S. Guo, S. Chen, L. Zhang, Y.F. Chen, K. Yao, Plastic Strain Determination With Nonlinear Ultrasonic Waves Using In Situ Integrated Piezoelectric Ultrasonic Transducers, *IEEE Transactions on Ultrasonics, Ferroelectrics, and Frequency Control* 65(1) (2018) 95-101.

[12] S. Guo, L. Zhang, M.S. Mirshekarloo, S. Chen, Y.F. Chen, Z.Z. Wong, Z. Shen, H. Liu, K. Yao, Method and analysis for determining yielding of titanium alloy with nonlinear Rayleigh surface waves, *Materials Science and Engineering: A* 669 (2016) 41-47.

[13] D. Chen, H. Xiao, J. Xu, An improved Richardson-Lucy iterative algorithm for C-scan image restoration and inclusion size measurement, *Ultrasonics* 91 (2019) 103-113.

[14] S. Guo, S. Chen, L. Zhang, W.H. Liew, K. Yao, Direct-write piezoelectric ultrasonic transducers for pipe structural health monitoring, *NDT & E International* 107 (2019) 102131.

[15] Y. Lu, L. Ye, Z. Su, Crack identification in aluminium plates using Lamb wave signals of a PZT sensor network, *Smart Materials and Structures* 15(3) (2006) 839-849.

[16] X. Zhao, H. Gao, G. Zhang, B. Ayhan, F. Yan, C. Kwan, J.L. Rose, Active health monitoring of an aircraft wing with embedded piezoelectric sensor/actuator network: I. Defect detection, localization and growth monitoring, *Smart materials and structures* 16(4) (2007) 1208.

[17] M. Li, X. Li, C. Gao, Y. Song, Acoustic microscopy signal processing method for detecting near-surface defects in metal materials, *NDT & E International* 103 (2019) 130-144.

[18] Z. Zhang, S. Guo, Q. Li, F. Cui, A.A. Malcolm, Z. Su, M. Liu, Ultrasonic detection and characterization of delamination and rich resin in thick composites with waviness, *Composites Science and Technology* (2020) 108016.

[19] J. Herrmann, J.-Y. Kim, L.J. Jacobs, J. Qu, J.W. Littles, M.F.J.J.o.A.P. Savage, Assessment of material damage in a nickel-base superalloy using nonlinear Rayleigh surface waves, *Ultrasonics* 44(12) (2006) 124913.

[20] Z. Zhou, K. Zhang, J. Zhou, G. Sun, J. Wang, Application of laser ultrasonic technique for non-contact detection of structural surface-breaking cracks, *Optics & Laser Technology* 73 (2015) 173-178.

- [21] M. Duquennoy, M. Ouaftouh, J. Deboucq, J.-E. Lefebvre, F. Jenot, M.J.A.P.L. Ourak, Influence of a superficial field of residual stress on the propagation of surface waves—Applied to the estimation of the depth of the superficial stressed zone, *101(23)* (2012) 234104.
- [22] A. Karabutov, N. Podymova, Quantitative analysis of the influence of voids and delaminations on acoustic attenuation in CFRP composites by the laser-ultrasonic spectroscopy method, *Composites Part B: Engineering* 56 (2014) 238-244.
- [23] A. Karabutov, N. Podymova, Nondestructive porosity assessment of CFRP composites with spectral analysis of backscattered laser-induced ultrasonic pulses, *Journal of Nondestructive Evaluation* 32(3) (2013) 315-324.
- [24] G. Wissmeyer, M.A. Pleitez, A. Rosenthal, V. Ntziachristos, Looking at sound: optoacoustics with all-optical ultrasound detection, *Light: Science & Applications* 7(1) (2018) 53.
- [25] X. Zhang, J.R. Fincke, C.M. Wynn, M.R. Johnson, R.W. Haupt, B.W. Anthony, Full noncontact laser ultrasound: first human data, *Light: Science & Applications* 8(1) (2019) 119.
- [26] J. Herrmann, J.-Y. Kim, L.J. Jacobs, J. Qu, J.W. Littles, M.F. Savage, Assessment of material damage in a nickel-base superalloy using nonlinear Rayleigh surface waves, 99(12) (2006) 124913.
- [27] X. Jian, Y. Fan, R. Edwards, S. Dixon, Surface-breaking crack gauging with the use of laser-generated Rayleigh waves, *Journal of applied physics* 100(6) (2006) 064907.
- [28] S. Dixon, B. Cann, D.L. Carroll, Y. Fan, R.S. Edwards, Non-linear enhancement of laser generated ultrasonic Rayleigh waves by cracks, *Nondestructive Testing and Evaluation* 23(1) (2008) 25-34.
- [29] A. Moura, A.M. Lomonosov, P. Hess, Depth evaluation of surface-breaking cracks using laser-generated transmitted Rayleigh waves, *Journal of Applied Physics* 103(8) (2008) 084911.
- [30] K. Li, Z. Ma, P. Fu, S. Krishnaswamy, Quantitative evaluation of surface crack depth with a scanning laser source based on particle swarm optimization-neural network, *NDT & E International* 98 (2018) 208-214.
- [31] H. Cho, S. Ogawa, M.J.N. Takemoto, E. International, Non-contact laser ultrasonics for detecting subsurface lateral defects, 29(5) (1996) 301-306.
- [32] C. Wang, A. Sun, X. Yang, B.-F. Ju, Y.J.J.o.A.P. Pan, Laser-generated Rayleigh wave for width gauging of subsurface lateral rectangular defects, 124(6) (2018) 065104.
- [33] A. Kromine, P. Fomitchov, S. Krishnaswamy, J. Achenbach, Laser ultrasonic detection of surface breaking discontinuities: scanning laser source technique, (2000).
- [34] I. Arias, J.D. Achenbach, A model for the ultrasonic detection of surface-breaking cracks by the scanning laser source technique, *Wave Motion* 39(1) (2004) 61-75.
- [35] Y. Sohn, S. Krishnaswamy, Interaction of a scanning laser-generated ultrasonic line source with a surface-breaking flaw, *The Journal of the Acoustical Society of America* 115(1) (2004) 172-181.